ELSEVIER

Journal of Structural Geology 27 (2005) 343–355

JOURNAL OF STRUCTURAL GEOLOGY

www.elsevier.com/locate/jsg

Structural features of an active strike-slip fault on the sliding flank of Mt. Etna (Italy)

Valerio Acocella[a,*], Marco Neri[b]

[a]*Dip. Scienze Geologiche Roma TRE. Largo S.L. Murialdo, 1, 00146 Roma, Italy*
[b]*Istituto Nazionale di Geofisica e Vulcanologia, Piazza Roma 2, 95123 Catania, Italy*

Received 9 May 2003; received in revised form 12 July 2004; accepted 20 July 2004
Available online 7 December 2004

Abstract

The strike-slip Pernicana fault system (PFS) was activated along the eastern flank of Mt. Etna during an earthquake in September 2002 and, one month later, during the eruption of the NE Rift. Structural and volcanological data suggest that the PFS was activated as a result of the slide of the NE flank of Etna. This activation produced surface fracturing on walls and on paved and unpaved roads. The segments of the PFS, arranged in a right stepping en échelon configuration, show (a) an inverse proportion between length and frequency; (b) fractal behavior over scales of 10^{-2}–10^{1} m, between their length, overstep and overlap; (c) consistent strike with regard to their fault array; and (d) a progressive eastward decrease in the displacement, along the smallest faults. The consistent geometric and kinematic features of the PFS, related to the sector collapse of Etna, are similar to those of faults in strike-slip settings.

Keywords: Active faulting; Strike-slip faults; Fractal behavior; Volcano collapse; Mt. Etna; Pernicana fault system

1. Introduction

Fault zones usually consist of closely-spaced fractures, formed through repeated tectonic events (e.g. Scholz, 1990). Since most of the segments are linked, these fault zones mainly give information on the advanced and/or mature stage of evolution of a fault zone.

Several studies have been made on fault zones developed during a single rupture, where most of the linkage through the segments has yet to occur; this usually occurs for small displacements of the faults affecting undeformed rocks or deposits. The best-known cases of fault zones developed in a single rupture consist of surface fractures related to earthquakes (e.g. Angelier and Bergerat, 2002; Angelier et al., 2003; Bergerat et al., 2003) or to episodes of magmatic activity (e.g. Rubin and Pollard, 1988; Billi et al., 2003; Lanzafame et al., 2003). These types of fault zones may give information on the very early stages of development of a fault zone, such as its formation, revealed by the spatial configuration of the fault segments and their possible processes of interaction (e.g. Koukouvelas et al., 1999; Acocella et al., 2000). The possibility to observe the continuous development of a fault zone, from its growth to its final development, is commonly achieved through experimental (Cox and Scholz, 1988; An and Sammis, 1996a; An, 1998) or numerical models (Segall and Pollard, 1980; Olson and Pollard, 1991; An and Sammis, 1996b; Willemse, 1997; Gupta and Scholz, 2000).

The 2002–2003 Etna eruption and its associated events permitted observation of the activation of an ~18-km-long active strike-slip fault, the Pernicana fault system (Acocella et al., 2003; Neri et al., 2004), mainly on paved and unpaved roads on the flank of the volcano. The different amounts of displacement along the fault, decreasing eastward by one order of magnitude, also gives the rare opportunity to appreciate and compare the growth of portions of the same structure.

In this work, we summarize the main structural features related to the development of this fault zone.

* Corresponding author. Tel.: +39-06-54888027; fax: +39-06-54-888201
E-mail addresses: acocella@uniroma3.it (V. Acocella), neri@ct.ingv.it (M. Neri).

0191-8141/$ - see front matter © 2004 Elsevier Ltd. All rights reserved.
doi:10.1016/j.jsg.2004.07.006

2. Geological background

The active fault developed during the 2002–2003 Etna eruption is located along the Pernicana fault system (PFS in Fig 1), one of the longest faults and most active in the Etnean area (Neri et al., 1991; Groppelli and Tibaldi, 1999). Mt. Etna is an active basaltic volcano located in eastern Sicily, at the front of the Apennine–Maghrebian Chain (Lanzafame et al., 1997; Fig. 1).

Volcanic activity at Mt. Etna is either focused at its four summit craters or occurs from fissures that are mainly concentrated in three so-called rift zones (Garduño et al., 1997; Behncke and Neri, 2003): the NE Rift, the S Rift and the W Rift (Fig. 1). Several studies present evidence for large scale sliding of the eastern and southern sectors of the volcano towards the E and S, respectively (Neri et al., 1991; Borgia et al., 1992, 2000; Lo Giudice and Rasà, 1992; Rust and Neri, 1996; Garduño et al., 1997; Froger et al., 2001;

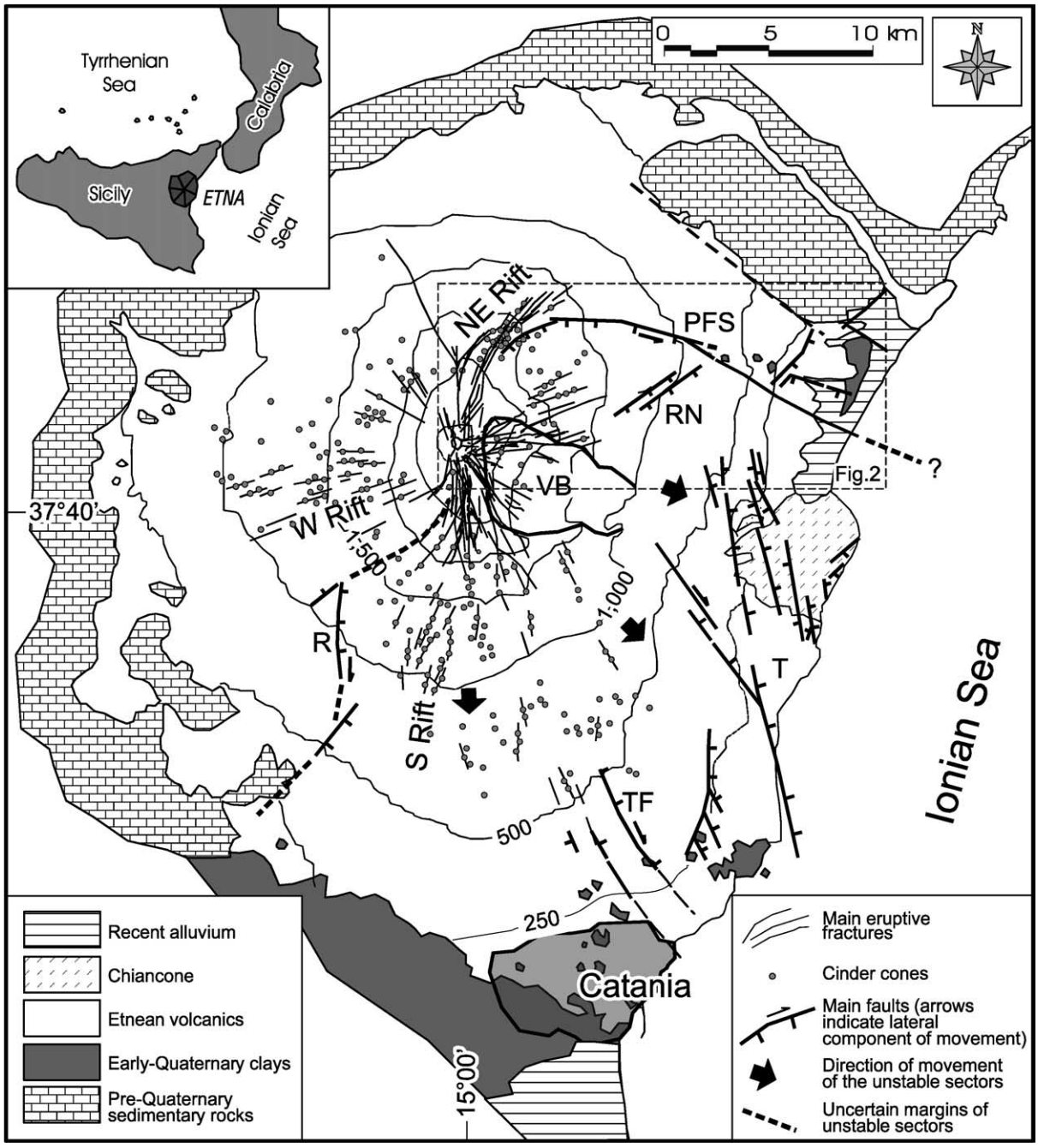

Fig. 1. Geological and tectonic map of Mount Etna. The boundaries of the unstable sector of the volcano are taken from Borgia et al. (1992) and Rust and Neri (1996). The sedimentary basement is made up of units of the Apenninic–Maghrebian Chain (North and West) and of early Quaternary clays (South). VB = Valle del Bove; PFS = Pernicana fault system; RN = Ripe della Naca Faults; T = Timpe Fault System; TF = Trecastagni–Mascalucia Faults; R = Ragalna Faults.

Acocella et al., 2003). The mobile eastern portion is bordered, to the north, by the E–W-trending PFS, with a left lateral-normal motion, mainly determined through field data (Fig. 1; Neri et al., 1991; Garduño et al., 1997). The sliding southern sector is bounded, at its western margin, by the N–S-trending Ragalna fault system, with a predominant dextral–normal motion (Fig. 1; Rust and Neri, 1996). The eastward and southward collapsing areas are separated by the Mascalucia and Trecastagni NW–SE-trending faults, with a normal to dextral displacement (Fig. 1; Lo Giudice and Rasà, 1992; Froger et al., 2001).

The extent of sliding of Mt. Etna at the surface and at depth is debatable, with detachments possibly ranging between 1–2 km above sea level (a.s.l.) (Bousquet and Lanzafame, 2001) and 6 km below sea level (b.s.l.) (Borgia et al., 1992). Recent studies suggest that both a shallow and a deep décollement may occur at the same time (Tibaldi and Groppelli, 2002).

The transtensive E–W-trending PFS (Fig. 1) develops eastward from the NE Rift (from 1850 m a.s.l.) to the coastline, over a distance of ~18 km (Neri et al., 2004). The PFS is partly characterized by a scarp, with a maximum morphological height of 70–80 m between 1000 and 1500 m a.s.l. At lower elevations (starting from 800 to 700 m a.s.l.), the PFS has a less defined morphological expression and is characterized by sinistral right-stepping faults.

Moderate surface deformation, characterized by creep processes with sinistral displacements ~2 cm/yr, has been occurring along the central portion of the PFS in the last decades (Obrizzo et al., 2001; Neri et al., 2004). This deformation has, at times, been accompanied by shallow (<2 km) and moderate seismic activity (2<M<3.5) (Azzaro et al., 1998).

The PFS is kinematically connected to the episodic opening and eruptions of the nearby NE Rift (Neri et al., 1991; Garduño et al., 1997; Tibaldi and Groppelli, 2002; Acocella and Neri, 2003; Acocella et al., 2003). In spite of this relationship, the central portion of the PFS has shown fairly continuous activity, with surface fracturing and seismic activity (1984–1988), also occurring in periods (1947–2002) when no eruptions occurred from the NE Rift.

3. Timing of events related to the development of the PFS during 2002–2003

On 22 September 2002, an earthquake (Md=3.7, focal depth=5 km b s.l.; INGV Mednet, 2003) occurred along the westernmost part of the PFS, with the epicenter at 1450 m a.s.l. This was accompanied by ground fracturing, with left-lateral displacement of 0.48 m, along the PFS, near Piano Provenzana (point 3 on Fig. 2).

At 20:25 GMT on 26 October, a seismic swarm (hypocenters between 1 and 6 km b.s.l.) affected the upper eastern flank of Mt. Etna (Patanè, 2002; Acocella et al., 2003). Early on 27 October, two eruptive fissure systems opened on the S and NE flanks. A 1000-m-long, N–S-trending eruptive fissure opened on the upper south flank, at 2850–2600 m a.s.l. and was active until the end of January 2003. Contemporaneously, NE–SW-trending eruptive fissures, ~4 km long, developed on the NE flank, from 3010 m a.s.l. to the lower NE Rift, at 1890 m a.s.l. (Fig. 2); the opening directions of these fissures are also shown in Fig. 2. This NE–SW-trending eruptive system was active for 7 days. Petrochemical data on the basalts erupted from the NE Rift show that the eruption was fed by residual magma within the summit conduit (Andronico et al., 2005), which migrated towards the NE Rift.

Contemporaneously during the opening of the NE Rift, the westernmost PFS moved by ~0.6 m, reaching, at the end of October, a total left-lateral displacement of ~1.1 m. On 12 November, displacement along the westernmost PFS totaled >1.25 m since the September earthquake (Fig. 3). At this time, the deformation propagated eastwards, with a decreasing left-lateral displacement, to the ~18 km distant coastline. The deformation was characterized by WNW–ESE-trending fault fractures with a right-stepping configuration, affecting roads, walls, buildings and railway lines. These fractures showed predominant left-lateral shear, with minor normal displacement and a dilational component.

In situ measurements of surface deformation along the PFS, aimed at evaluating the geometry, kinematics and evolution of the faults, were carried out twice per week between September 2002 and February 2003. These revealed that different portions moved at different times. The time variations of the left-lateral component of displacement along portions of the PFS are shown in Fig. 4. The deformation propagated from west to east: it started from the NE Rift area and then migrated to the eastern PFS. The western PFS was mostly active between the 22 September earthquake and the beginning of November and almost stopped moving 40–50 days before the eastern portion did. Conversely, activity at the eastern PFS was mainly concentrated between the end of October and the beginning of November, continuing, with displacements of 0.01–0.001 m/month, until November 2003.

4. Structural features of the PFS developed during the 2002–2003 eruption

Compared with the limited portions of the moderately active (displacements of cm/yr) PFS in the last decades, the sudden activation of the entire PFS during 2002–2003 shows much higher displacement rates (m/yr) and is easily recognizable. Therefore, the sudden fracturing along the PFS permitted: (a) the study of the 2002–2003 deformation along the undeformed portions of the fault; and (b) the chance to clearly discriminate, where the PFS was previously active, the deformation pattern related to the 2002–2003 events.

Investigations were mainly made on previously

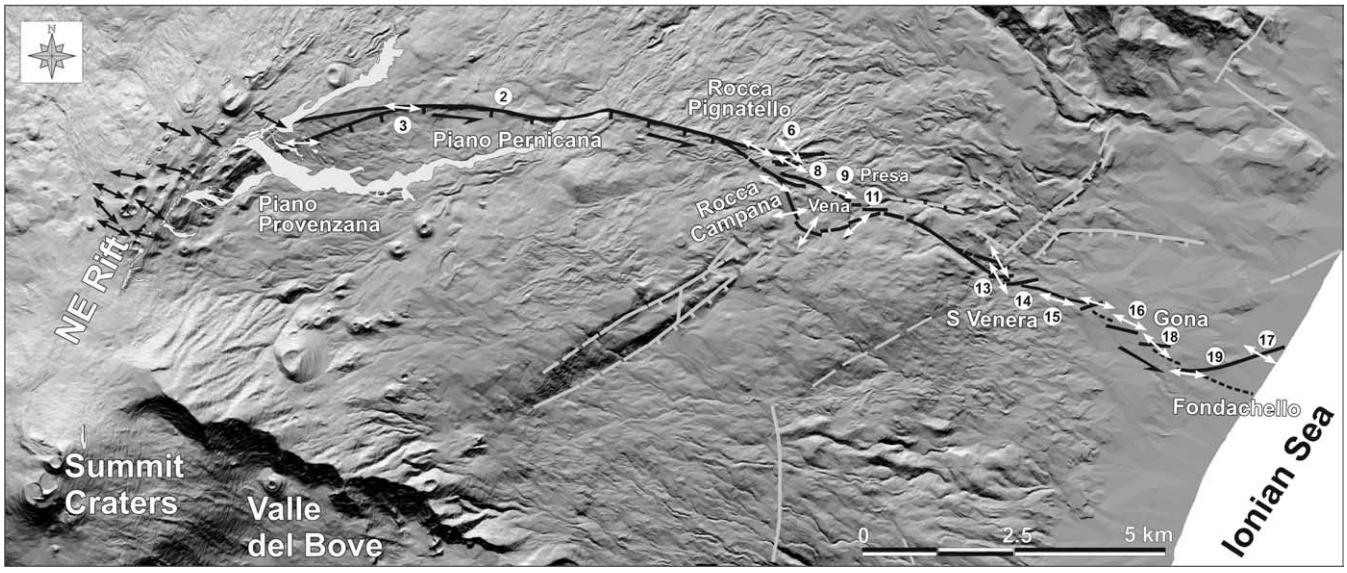

Fig. 2. Digital elevation model of the NE part of Mt. Etna, showing the left-lateral Pernicana fault system (PFS, in black) developed during 2002–2003, from the NE Rift to the Ionian coastline. Numbers indicate measurement sites; double white arrows represent the opening direction of the dilational faults along the PFS, black double arrows represent the opening direction of the eruptive fissures along the NE Rift, as obtained during the 2002 eruption. The lava flows of the 2002 eruption (in light gray) are also shown.

undeformed man-made structures; these consisted of buildings and paved and unpaved roads which have been repaired since the last slip event accompanied by ground fracturing in 1988. A minor amount of data was taken from unpaved roads, soils and rocky areas. These investigations therefore permitted analysis of formation of new surface ruptures, related to the reactivation of the PFS (Neri et al., 2004).

A feature of the PFS during the 2002–2003 eruption is the segmentation of the fault zone at the surface. The ~18-km-long PFS is characterized by an array of segments arranged in a right-stepping en échelon configuration at different scales, at least within the range 10^{-2}–10^{1} m (Fig. 5). The main geometric features of these fault segments, such as their length, overstep, overlap and their angle with regard to their array, are defined in Fig. 6. The values of these geometric features, as well as the kinematic features of the fault segments (horizontal, vertical and dilational components of displacement and the resulting opening directions) are listed in Table 1.

The overall PFS has a mean ~N110°E trend, but its single segments, whatever their length, show a mean N79°E trend (Fig. 7a). The discrepancy between the trend of the overall PFS and the mean trend of its component segments can be explained by the repeated right-stepping en échelon configuration of the fault segments. The fault segments are

Fig. 3. Photograph of the westernmost part of the PFS (site 3 in Fig. 2), where the left-lateral displacement in early November totaled > 1.25 m. The photograph shows an uplifted area within a restraining bend, made by two interacting underlapping ~E–W-trending left-lateral faults, along a paved road.

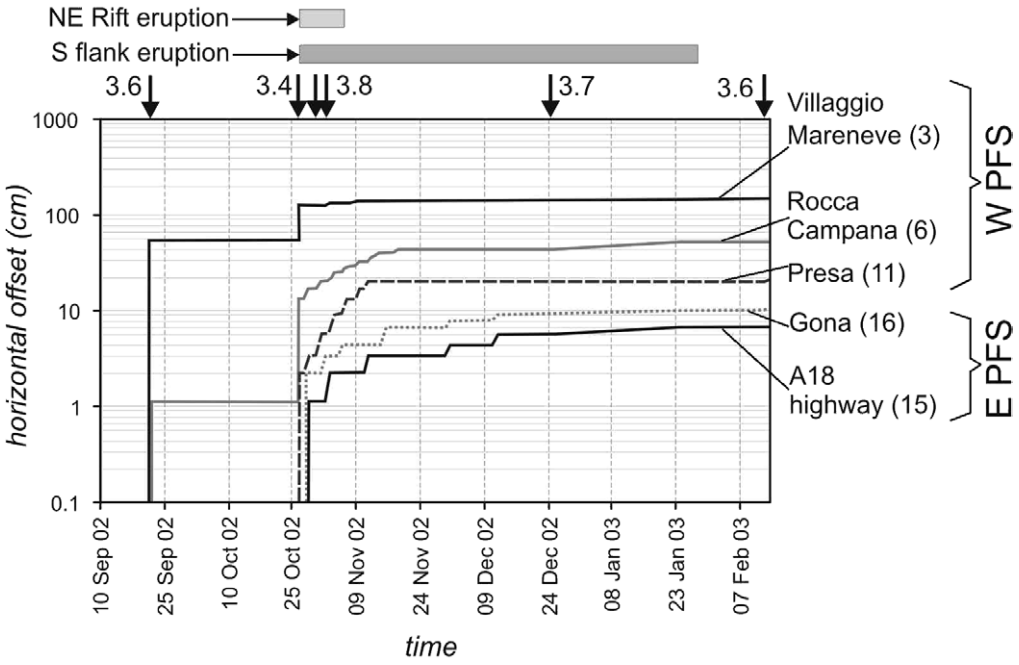

Fig. 4. Variation of the left-lateral displacement with time along portions of the PFS (site numbers are shown in Fig. 2). The arrows on top of diagram refer to the occurrence of major (magnitude in numbers) earthquakes along the PFS.

at angles of 6–35° to the strike of the fault zone (Fig. 7b). The clustering of the orientations of the fault segments around a few preferred values (Fig. 7a) can be similarly explained by the fact that every fault segment, at different scales, is made up of smaller en échelon segments.

Two faults are here defined as interacting when they show curved tips while approaching each other, as a consequence of the exerted stress changes (interaction stage). The interaction process eventually leads to the geometric connection of the segments, forming a continuous, sinuous structure (linkage stage).

The western PFS consists of progressively larger

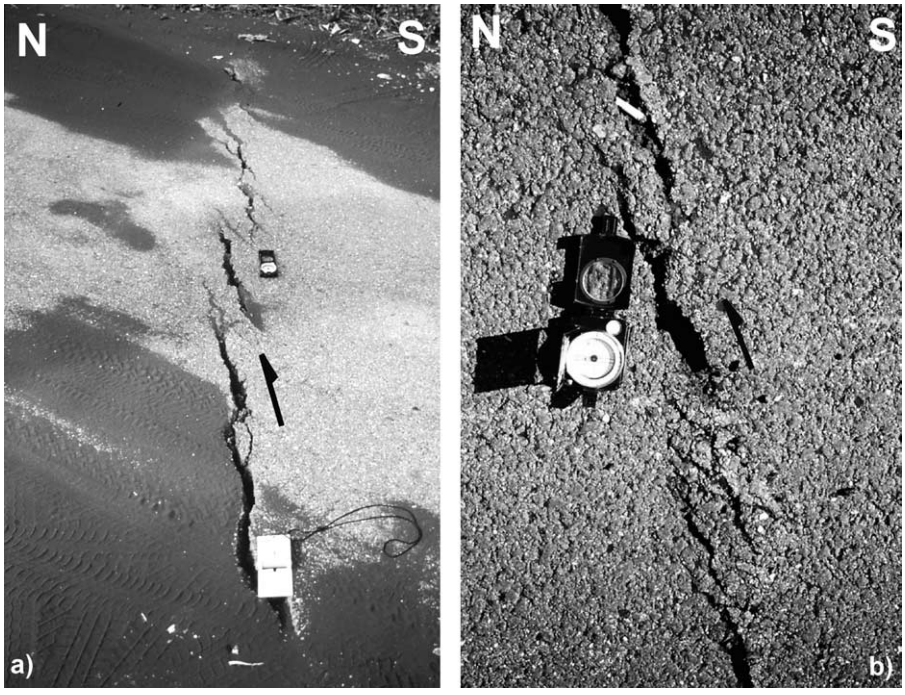

Fig. 5. Examples of ~E–W-trending left-lateral fault segments in a dextral en-échelon configuration, at different scales along portions of the PFS: (a) site 14; (b) site 16 (see Fig. 2 for the locations of the sites). Compasses are oriented parallel to the opening direction of the faults, highlighting their predominant left-lateral component of motion.

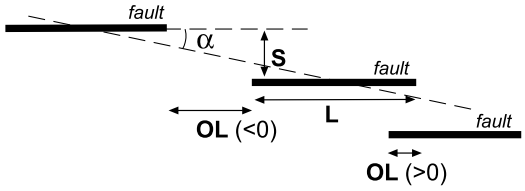

Fig. 6. Definition of the geometrical parameters associated with the faults segments composing the PFS. Map view: L=length of segment; S=overstep between segments; OL=overlap between segments (negative values indicate underlapping, positive values indicate overlapping); α=angle between the trend of the segment and the trend of the array to which it belongs.

interacting segments becoming linked westwards. The size distribution of these segments can be appreciated in Fig. 8, which indicates that, for the measured range of faults, smaller faults (eastern PFS) are much more common than the larger ones (western PFS).

Leaving aside the degree of interaction of the segments, the surface fractures along the PFS show a consistency, at different scales, between their spatial features. There is a correlation between the mean length of the faults (L) and their overstep (S), regardless of their dimensions (between 10^{-2} and 10^{1} m) (Fig. 9a); the greater the length of the nearby faults, the larger their separation. A mean ratio of 8:1 between the total length of the faults and their overstep can be derived from the best-fit line in Fig. 9a. This ratio is similar to the 10:1 proposed as the threshold under which linkage through strike-slip segments can occur (An, 1997).

The data also show the correlation between the mean length of the faults (L) and their overlap (OL), regardless of their dimensions (between 10^{-2} and 10^{1} m) (Fig. 9b). The fact that the overlap values are mostly negative indicates the prevalence of an underlapping configuration between fault segments. Fig. 9b indicates that, the greater the length of nearby faults, the larger their underlap. The OL:S ratio of the fault segments is ~1. This value is rather lower than the mean value (~4.7) found for overlapping and underlapping strike-slip faults worldwide (Aydin and Schultz, 1990).

The variations between the overstep and the overlap among the fault segments also show, as may be expected comparing Fig. 9a and b, a similar correlation (Fig. 9c). Therefore, Fig. 9a–c shows that, regardless of the dimensions, there is a consistency in the relationships among the spatial features (length, overstep and overlap) of the fault segments along the PFS.

The ~E–W-trending fault segments along the PFS are consistent with a left-lateral transtension. The variations in the horizontal, vertical and dilational components of displacement of the fault segments are shown in Fig. 10

Table 1
Main geometric and kinematic features of the ~E–W-trending surface faults along the PFS. The locations of the sites are reported in Fig. 2

Site	Segment length (L) (m)	Segment overstep (S) (m)	Segment overlap (OL) (m)	Segment trend (°)	Array trend (°)	Left-lateral component (m)	Normal component (m)	Dilational component (m)	Opening direction (°)
2	25±8	6±2	−6±2	N70±15		0.53	0.2	0.14	N96±14
2	0.35±0.1	1±0.3	−1.5±0.5						
3	36±5	8±1	−8±0.5	N70	N91	1.25	0.6	0.58	N90±15
6				N98		0.4		0.09	N145±25
6	0.8±0.15	0.3±0.5	0.2±0.5						
8	0.15±4	0.07±0.02	0.06±0.02						
8				N80	N95	0.25	0.04		N140±20
8	0.6±0.2	0.2±0.4	0±0.1					0.07	
9	1.5±0.3	0.2±0.04	0±0.1			0.35			
9				N100		0.05		0.04	N135
11	20±5	5.5±1		N70±20		0.2	0.03		N135
11	0.45±0.1	0.15±0.04	0.05±0.01	N52	N82	0.035		0.035	N100
11				N90	N108				
11				N55	N90				
13	1.5±0.3	0.3±0.05	0.1±0.5	N58	N80	0.06	0.01		N145±3
13				N60	N77			0.02	
14	0.25±0.05	0.15±0.04	−0.12±0.03	N59±2	N65	0.025	0	0.015	N89±2
15	0.25±0.06	0.06±0.01	0±0.1	N81	N115	0.05			N100
15	0.7±0.012	0.12±0.02	0±0.1	N80	N108				
16	0.75±0.08	0.15±0.05	−0.15±0.03	N80	N100				
16	0.52±0.05	0.11±0.02	−0.15±0.04	N104		0.05	0	0.02	N166
16	0.25±0.06	0.15±0.03	−0.15±0.03	N78	N90			0.01	N102
17	0.22±0.04	0.1±0.02	−0.11±0.02	N68		0.04	1.5	0.01	N70
18				N78	N96	0.015	0	0.01	N156
18	0.75±0.09	0.2±0.04	−0.08±0.02	N82	N93	0.025	0		N138
18	2±0.2	0.75±0.01	−0.4±0.07	N81	N92				
19	0.52±0.08	0.1±0.02	−0.1±0.02	N80	N89	0.07	0	0.015	N105±7
19				N82	N94				
19				N81	N96				

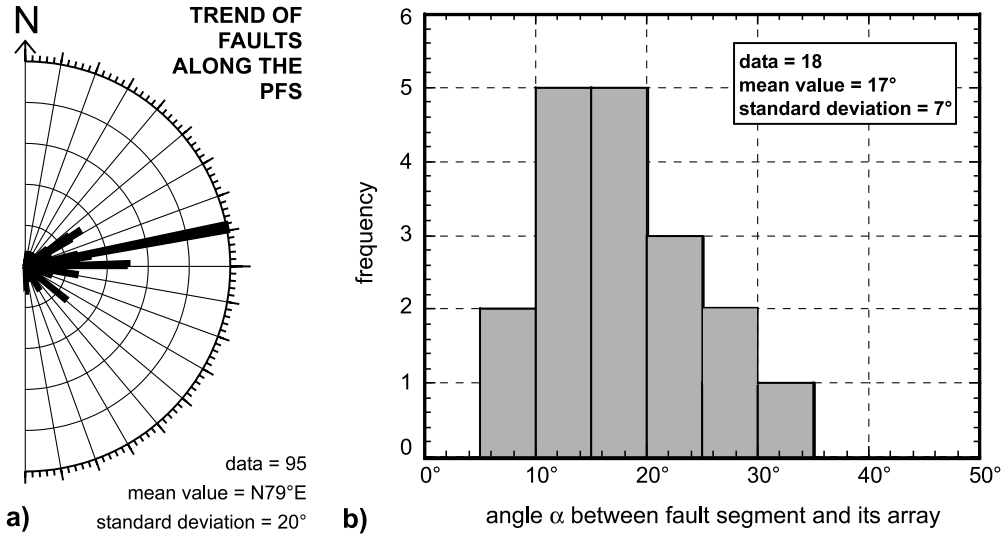

Fig. 7. (a) Strike of the fault segments along the PFS. (b) Distribution of the angle α, at different scales, along the ~E–W-trending systems of the PFS.

as a function of the eastward distance from the axis of the NE Rift. The left-lateral component is much larger at all points than the normal and dilational components, showing the prevalence of the strike-slip motion.

The maximum displacements are observed in the western PFS, at site 3; further to the west, the PFS is buried under the products of the 2002 eruption of the NE Rift. The left-lateral, normal and dilational components in Fig. 10 show a marked decrease eastward, indicating that the PFS moved with a largely asymmetric slip. The overall transtensional component found along the PFS is summarized in the inset of Fig. 10, which associates the mean opening direction (the single values are reported in Fig. 2 and in Table 1) of the faults on the field with their mean direction (Fig. 7).

The positive correlation between the length of the faults and their left-lateral component of displacement is shown in Fig. 11. This relation shows how the larger faults are associated with the larger left-lateral slips; both the slip and the length of the faults increase westwards along the PFS, where linkage has been observed.

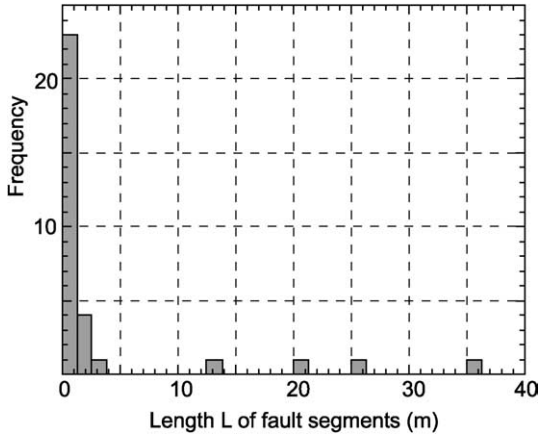

Fig. 8. Distribution of the length L of the fault segments along the PFS.

In addition to the ~E–W-trending faults, two minor fault systems, both kinematically consistent with the left-lateral displacement of the PFS, also occur. These systems consist of (a) N130°-trending transtensive dextral faults and (b) N–S-trending thrust faults.

(a) The N130°-trending faults (Fig. 7) are observed on the central-western portion of the PFS, in the area of the sites 6, 8 and 9. These consist of dextral faults, with a minor extensional component. Their displacement is usually one order of magnitude smaller (that is, very few centimeters) with regard to the left-lateral ~E–W-trending faults to which they are associated. The acute angle between the dextral and sinistral set is $50 \pm 20°$.
(b) The N–S-trending thrust faults are observed in the area of site 11. These are low-angle faults (Fig. 12a), which form in the restraining zones between right-stepping left-lateral segments (Fig. 12b). Compressional features, such as open (interlimb angle $>150°$) folds a few meters wide or thrusts with displacement of a few tens of centimeters, are also observed in similar restraining bends along the westernmost PFS (sites 2 and 3), where the interaction between the fault segments is stronger (Fig. 3).

5. Discussion of the observed deformation pattern along the PFS

Surface fracturing, with a maximum horizontal displacement ~0.5 m, along the western PFS was first triggered by the September 2002 earthquake The earthquake was followed, one month later, by the activation of eruptive fissures along the NE Rift, with the extrusion of magma within the summit conduit. During the eruption, the PFS moved again, increasing its displacement (up to ~2 m) in

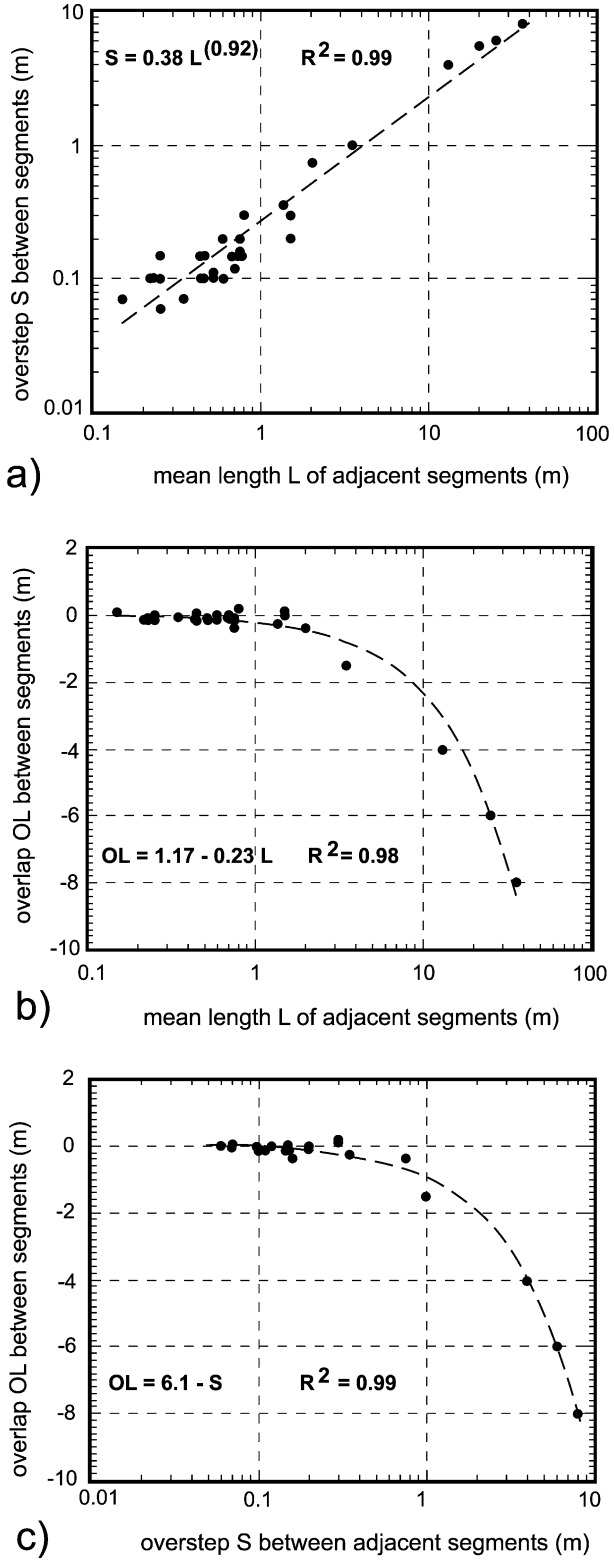

Fig. 9. Correlations among the geometric features of adjacent fault segments along the PFS, at all the measured scales. (a) Length *L* vs. overstep *S*. (b) Length *L* vs. overlap *OL*. (c) Overstep *S* vs. overlap *OL*.

the former epicenter area and propagating eastwards, to the coastline.

These events show a kinematic connection between the NE Rift and the PFS. Such a connection is also highlighted by the consistency in the opening directions between the fissures of the NE Rift (black double arrows) and the faults of the PFS (white double arrows) (Fig. 2). Activity along the PFS may have enhanced the opening of the NE Rift and the related eruption of magma; these, in turn, may have induced larger deformations on the PFS. Within this framework, the PFS may play a double role: (a) its movement creates the space and the decompression for the rise of magmas along the NE Rift; and (b) it accommodates the opening of the NE Rift and the eastward slide of the eastern portion of the volcano. This connection between the PFS and the NE Rift results in a strong link between sliding and volcanic activity on the NE flank of Mt. Etna (Acocella et al., 2003; Neri et al., 2004). Even though this link was previously proposed (Froger et al., 2001, and references therein), the 2002–2003 eruption permitted the observation and demonstration of the occurrence of lateral slip of the eastern flank of Mt. Etna during an eruption (Acocella et al., 2003; Neri et al., 2004).

Surface fracturing along the PFS consists of left lateral fault segments with a right-stepping en échelon configuration, mainly displaying $6° < \alpha < 35°$ (Fig. 7b); these segments may thus be interpreted as Riedel systems (*R*) of the developing PFS shear zone (e.g. Sylvester, 1988). Conversely, the ~NW–SE-trending dextral faults can be interpreted as antithetic Riedel systems of the PFS (i.e. Sylvester, 1988). The Riedel shears are both interacting and linking along the PFS. The fault segments are linked on the westernmost PFS, producing mostly continuous fault segments; conversely, they are still in the form of interacting separate segments on the easternmost PFS, where the displacement is lower (Fig. 10).

The ratio between the total length of the fractures and their overstep has been used to evaluate a priori the possibility of linkage between fractures in strike-slip (An, 1997) and extensional (Acocella et al., 2000) settings. Values of the total length/spacing of >10 have been inferred to promote the interaction, whereas the interaction is inhibited for ratios of <10; this threshold is determined by the possibility that the stress changes associated with each interacting fault reach the opposite fault.

The mean ratio of 8:1 between the total length of the fractures and their overstep is quite close to the estimated threshold and therefore does not permit strong insights on the tendency of the fractures to interact. Nevertheless, a limited interaction is expected among the faults with the lowest total length/spacing ratios, while a widespread interaction is expected among the faults with the highest total length/spacing ratios. Field observations show that interactions usually evolved toward linkages, progressively developing these features: (1) arcuate fault tips; (2) a discontinuous fault zone between the interacting faults; (3) a continuous, sinuous structure linking the two faults, usually

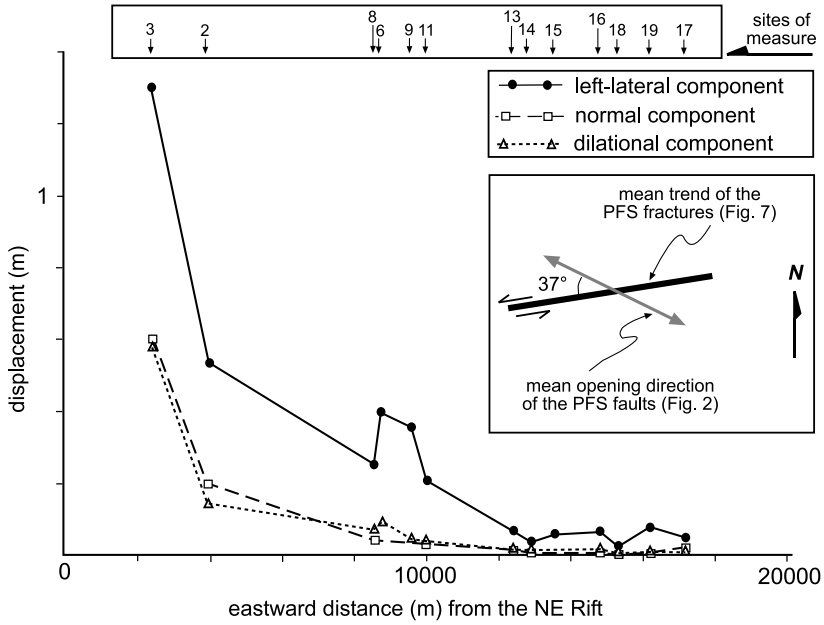

Fig. 10. Variation of the left-lateral, normal and dilational components of displacement at the sites along the PFS. Distances are calculated along a N110° direction eastward from the axis of the NE Rift. The lowermost inset shows the mean opening direction of the faults along the PFS compared with their mean trend.

characterized by a restraining bend between underlapping faults.

Most of the segments show an underlapping configuration, regardless of their interaction or linkage (Fig. 9b). Existing models (Segall and Pollard, 1980; Aydin and Schultz, 1990) of interaction of strike-slip faults interpret the underlapping configuration as the early stage of the interaction process, which rapidly produces an overlapping configuration. The fact that the underlapping configuration is also observed in the western PFS, where fault segments are linked, indicates that this configuration is independent of the interaction or linkage stage. The underlapping segments along the western PFS indicate that the overlapping configuration between segments is not the rule in a linkage process. Field data along strike-slip faults elsewhere (Aydin and Schultz, 1990) and analog models (An, 1998; McClay and Bonora, 2001) support this possibility. A similar small percentage of underlapping configurations have also been observed in numerical models of interacting normal faults (Willemse, 1997) and among interacting extension fractures and normal faults (Acocella et al., 2000). These data show that a limited number of underlapping interacting fractures occur both on strike-slip and extensional domains.

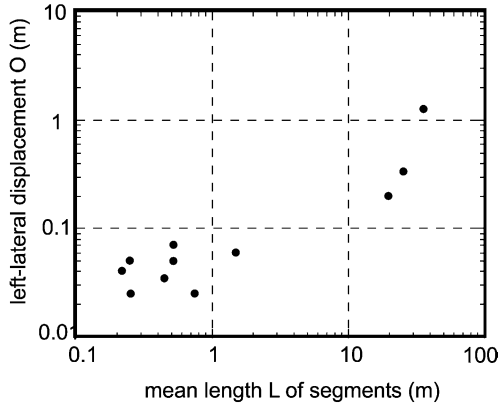

Fig. 11. Proportion between the mean length of the fault segments L along the PFS and their left-lateral component of displacement O.

Two hypotheses suggest an explanation for the underlapping configuration of the strike-slip segments at PFS. (a) The underlap may be controlled by pre-existing structures, such as the deeper portion of PFS. A similar mechanism was previously invoked for the reactivation of faults of the Somerset coast, England (Kelly et al., 1999). This mechanism, however, fails to explain why the deeper pre-existing PFS should also be underlapping. (b) The underlap may be related to the boundary stress conditions of PFS. The transtensive PFS is in fact largely controlled by the slide of the Etna flank and is not the direct consequence of a strike-slip setting. Thus, it can be expected that it forms under stress ($\sigma1$–$\sigma3$) lower than commonly associated with strike-slip settings. This lower $\sigma1$–$\sigma3$ may account for the development of shorter and underlapping fault segments. Similar variations in the geometry of strike-slip faults with the boundary tectonic conditions have been repeatedly observed (Kim and Sanderson, 2004, and references therein).

The spatial relationships between the fault segments, at the observed scales, suggest a consistency, as indicated by the constant proportions between their mean length, overstep and overlap (Fig. 9). Even though the data are limited (Fig. 9), this scale-independent consistency suggests a fractal behavior of the spatial configuration of the faults

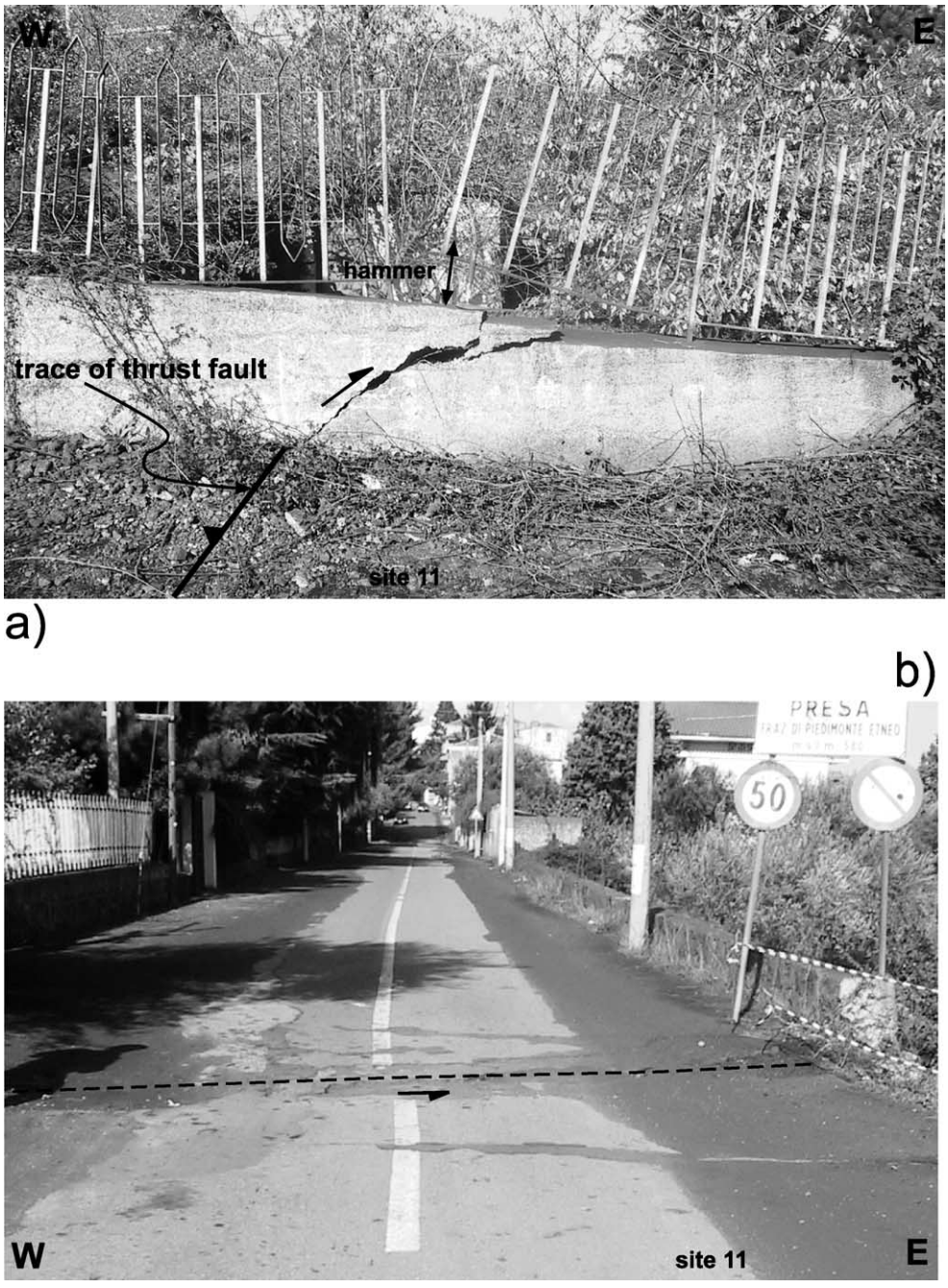

Fig. 12. (a) Photograph of a N–S-trending thrust fault along a wall near the town of Presa (site 11 in Fig. 2). The hammer in the center of the photograph provides a scale. This thrust fault connects splays of ~E–W-trending en-échelon segments of sinistral right-stepping faults. (b) Here, one of the ~E–W-trending left-lateral segments connected by the thrust fault is displacing the road with a left-lateral movement of ~0.2 m.

along the PFS, regardless of the interaction or linkage stage. As far as the overall configuration of interacting strike-slip faults is concerned, a scale independence of fault patterns (Tchalenko, 1970; Aviles et al., 1987; Okubo and Aki, 1987; Sornette and Davy, 1991; Poliakov and Herrmann, 1994) and pull-apart basins and pressure ridges (Aydin and Nur, 1982) has been proposed. Also, a relationship between fault length and the extent of the interaction zone was observed through 2D computer automation (An and Sammis, 1996b).

The measured components of displacements along the PFS show a marked eastward decrease, indicating that most of the displacement occurred in the highest part of the volcano. Both the horizontal and the vertical displacements show a proportion with the length of the faults, which is consistent with previous studies, also on normal faults (Dawers et al., 1993; Watterson et al., 1996, and references therein).

As shown in Fig. 1, the central and western parts of the

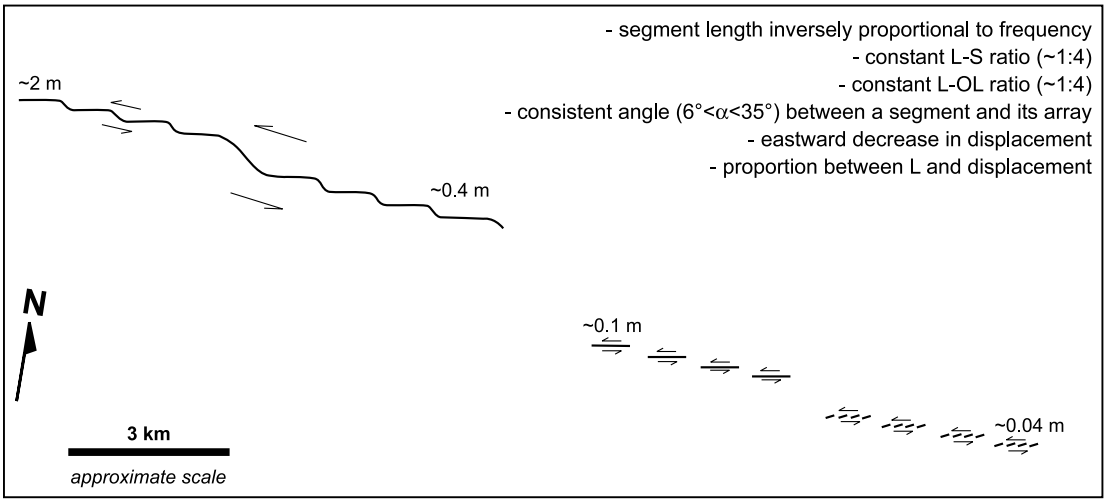

Fig. 13. Schematic model for the PFS during the 2002–2003 events. The consistency of the fault zone is shown by its geometric and kinematic features. Numbers refer to the measured amounts of displacement.

PFS are located within the volcanic pile, whereas the eastern PFS is mainly located on clay. The overall geometric and kinematic features of the PFS show consistent properties (Figs. 7–9) or constant variations at a broad scale (Fig. 10) and therefore do not seem to be significantly affected by abrupt changes in lithology or the presence of man-made structures; this suggests that the deformation pattern does not depend upon the substratum variations. Nevertheless, the longer-term evolution of the deformation along the PFS (Fig. 4) may depend upon the lithology. In fact, the monitoring along the portions of the PFS (Fig. 4) shows that, after early November 2002, movement of the western portion of the PFS, within the volcanic pile, decreased dramatically, while parts of the eastern portion, within the clay sediments, continued to creep.

The collected data do not allow the exclusion of the possibility that the fault zone may be segmented at surface and connected into a single fault at depth. Similar geometries of fractures splaying upwards have repeatedly been observed in nature (Pollard and Aydin, 1988, and references therein).

The geometry and kinematics of the newly-formed segments along PFS are summarized in Fig. 13. The variation in the spectrum of geometries and kinematics of the interacting segments may be explained by the concomitant occurrence of elastic and inelastic deformation in different parts of PFS. To the east, the interaction between isolated segments is mainly the result of an elastic process (Segall and Pollard, 1980). Conversely, to the west, the linkage experienced by the segments to form a continuous shear zone is the result of an inelastic process. Evolving fault segments within PFS must therefore experience elastic stress changes, during their interaction, prior to the inelastic processes that link them.

Moreover, in Fig. 13 the amount of segmentation along strike of PFS decreases with total displacement. This is interpreted as the result of the fact that the segments link towards the western portion, where displacement is higher.

The consistent geometric and kinematic features of PFS, as summarized in Fig. 13, are therefore in agreement with those of interacting and linking faults in strike-slip settings. This shows how structures resulting from gravitational and/or magmatic stresses may follow the same geometric and kinematic modalities of rupture as those subject to tectonic stresses.

6. Conclusions

Surface fracturing occurred along the PFS during the 2002–2003 Etna eruption The segments along the PFS are arranged in a right-stepping en-échelon configuration, with consistent relationships, at every measured scale, among their length, overstep and overlap. The kinematic features of the PFS show a progressive eastward decrease in the displacement, along the smallest faults.

These data show that strike-slip faults related to the slide of the Etna flank have consistent geometric and kinematic features. These are in broad agreement with those of interacting and linking faults in strike-slip settings. This similarity shows how structures related to gravitational and/or magmatic stresses may follow the same modality of rupture as those subject to tectonic stresses.

Acknowledgements

The authors thank B. Behncke and L. Lanzafame for useful comments and help in the fieldwork, and R.

Funiciello for his encouragement. This work was partly financed by GNDT funds (under the responsibility of C. Faccenna). The reviewers N. Dawers and D. Peacock are acknowledged for their useful comments, which improved the manuscript.

References

Acocella, V., Neri, M., 2003. What makes flank eruptions? The 2001 Mount Etna eruption and its possible triggering mechanisms. Bulletin of Volcanology 65, 517–529.

Acocella, V., Gudmundsson, A., Funiciello, R., 2000. Interaction and linkage of extensional fractures: examples from the rift zone of Iceland. Journal of Structural Geology 22, 1233–1246.

Acocella, V., Behncke, B., Neri, M., D'Amico, S., 2003. Link between large-scale flank slip and 2002–2003 eruption at Mt. Etna (Italy). Geophysical Research Letters 30 (24), 2286.

An, L., 1997. Maximum link distance between strike-slip faults: observations and constraints. Pure and Applied Geophysics 150, 19–36.

An, L.J., 1998. Development of fault discontinuities in shear experiments. Tectonophysics 293, 45–59.

An, L., Sammis, C.G., 1996a. Development of strike-slip faults: shear experiments in granular materials and clay using a new technique. Journal of Structural Geology 18, 1061–1077.

An, L., Sammis, C.G., 1996b. A cellular automaton for the development of crustal shear zones. Tectonophysics 253, 247–270.

Andronico, D., Branca, S., Calvari, S., Burton, M., Caltabiano, T., Corsaro, R.A., Del Carlo, P., Garfì, G., Lodato, L., Miraglia, L., Muré, F., Neri, M., Pecora, E., Pompilio, M., Salerno, G., Spampanato, L.A., 2005. Multi-disciplinary study of the 2002–03 Etna eruption: insights into a complex plumbing system. Bulletin of Volcanology, in press doi: 10.1007/S00445-004-0372-8.

Angelier, J., Bergerat, F., 2002. Behaviour of a rupture of the 21 June 2000 earthquake in South Iceland as revealed in an asphalted car park. Journal of Structural Geology 24, 1925–1936.

Angelier, J., Lee, J.C., Chu, H.T., Hu, J.C., 2003. Reconstruction of fault slip of the September 21st, 1999, Taiwan earthquake in the asphalted surface of a car park, and co-seismic slip partitioning. Journal of Structural Geology 25, 345–350.

Aviles, C.A., Scholz, C.H., Boatwright, J., 1987. Fractal analysis applied to characteristic segments of the San Andreas fault. Journal of Geophysical Research 92, 331–344.

Aydin, A., Nur, A., 1982. Evolution of pull-apart basins and their scale independence. Tectonics 1, 91–105.

Aydin, A., Schultz, A., 1990. Effect of mechanical interaction on the development of strike-slip faults within echelon patterns. Journal of Structural Geology 12, 123–129.

Azzaro, R., Branca, S., Giammanco, S., Gurrieri, S., Rasà, R., Valenza, M., 1998. New evidence for the form and extent of the Pernicana Fault System (Mt. Etna) from structural and soil-gas surveying. Journal of Volcanology and Geothermal Research 84, 143–152.

Behncke, B., Neri, M., 2003. Cycles and trends in the recent eruptive behaviour of Mount Etna (Italy). Canadian Journal of Earth Science 40, 1405–1411.

Bergerat, F., Angelier, J., Gudmundsson, A., Torfason, H., 2003. Push-ups, fracture patterns, and palaeoseismology of the Leirubakki Fault, South Iceland. Journal of Structural Geology 25, 591–609.

Billi, A., Acocella, V., Funiciello, R., Giordano, G., Lanzafame, G., Neri, M., 2003. Mechanism for ground surface fracturing and incipient slope failure associated to the July–August 2001 eruption of Mt. Etna, Italy: analysis of ephemeral field data. Journal of Volcanology and Geothermal Research 122, 281–294.

Borgia, A., Ferrari, L., Pasquarè, G., 1992. Importance of gravitational spreading in the tectonic and volcanic evolution of Mt. Etna. Nature 357, 231–235.

Borgia, A., Lanari, R., Sansosti, E., Tesauro, M., Berardino, P., Fornaro, G., Neri, M., Murray, J.B., 2000. Actively growing anticlines beneath Catania from the distal motion of Mount Etna's decollement measured by SAR interferometry and GPS. Geophysical Research Letters 27, 3409–3412.

Bousquet, J.C., Lanzafame, G., 2001. Nouvelle interprétation des fractures des éruptions latérales de l'Etna: conséquences pour son cadre tectonique. Bulletin de la Société Géologique de France 172, 455–467.

Cox, S.J.D., Scholz, C.H., 1988. On the formation and growth of faults: an experimental study. Journal of Structural Geology 10, 413–430.

Dawers, N.H., Anders, M.H., Scholz, C.H., 1993. Growth of normal faults: displacement–length scaling. Geology 21, 1107–1110.

Froger, J.L., Merle, O., Briole, P., 2001. Active spreading and regional extension at Mount Etna imaged by SAR interferometry. Earth and Planetary Science Letters 187, 245–258.

Garduño, V.H., Neri, M., Pasquarè, G., Borgia, A., Tibaldi, A., 1997. Geology of the NE Rift of Mount Etna, Sicily (Italy). Acta Vulcanologica 9, 91–100.

Groppelli, G., Tibaldi, A., 1999. Control of rock rheology of deformation style and slip-rate along the active Pernicana fault, Mt. Etna, Italy. Tectonophysics 305, 521–537.

Gupta, A., Scholz, C., 2000. A model of normal fault interaction based on observations and theory. Journal of Structural Geology 22, 865–879.

INGV Mednet, 2003. Terremoti in Italia e nel mondo registrati dalla rete Mednet, http://mednet.ingv.it/events/Welcome.html.

Kelly, P.G., Peacock, D.C.P., Sanderson, D.J., McGurk, A.C., 1999. Selective reverse reactivation of normal faults and deformation around reverse-reactivated faults in the Mesozoic of the Somerset coast. Journal of Structural Geology 21, 493–509.

Kim, Y.S., Sanderson, D.J., 2004. Similarities between strike-slip faults at different scales and a simple age determining method for active faults. The Island Arc 13, 128–143.

Koukouvelas, I.K., Asimakopoulos, M., Doutsos, T.T., 1999. Fractal characteristics of active normal faults: an example of the eastern Gulf of Corinth, Greece. Tectonophysics 308, 263–274.

Lanzafame, G., Leonardi, A., Neri, M., Rust, D., 1997. Late overthrust of the Appenine–Maghrebian Chain at the NE periphery of Mt. Etna, Italy. Comptes Rendus de Académie des Sciences de Paris 324, 325–332.

Lanzafame, G., Neri, M., Acocella, V., Billi, A., Funiciello, R., Giordano, G., 2003. Structural features of the July–August 2001 Mount Etna eruption: evidence for a complex magma supply system. Journal of the Geological Society of London 160, 531–544.

Lo Giudice, E., Rasà, R., 1992. Very shallow earthquakes and brittle deformation in active volcanic areas: the Etnean region as an example. Tectonophysics 202, 257–268.

McClay, K., Bonora, M., 2001. Analog models of restraining stopovers in strike-slip systems. AAPG Bulletin 85, 233–260.

Neri, M., Garduño, V.H., Pasquarè, G., Rasà, R., 1991. Studio strutturale e modello cinematico della Valle del Bove e del settore nord-orientale etneo. Acta Vulcanologica 1, 17–24.

Neri, M., Acocella, V., Behncke, B., 2004. The role of the Pernicana Fault System in the spreading of Mt. Etna (Italy) during the 2002–2003 eruption. Bulletin of Volcanology, 66, 417–430, doi: 10.1007/S00445-003-0322-X.

Obrizzo, F., Pingue, F., Troise, C., De Natale, G., 2001. Coseismic displacements and creeping along the Pernicana fault (Etna, Italy) in the last 17 years: a detailed study of a tectonic structure on a volcano. Journal of Volcanology and Geothermal Research 109, 109–131.

Okubo, P.G., Aki, K., 1987. Fractal geometry in the San Andreas fault system. Journal of Geophysical Research 92, 345–355.

Olson, J.E., Pollard, D.D., 1991. The initiation and growth of en echelon veins. Journal of Structural Geology 13, 595–608.

Patanè, D., 2002. Aggiornamento delle attività di monitoraggio sismico all'Etna: http://www.ct.ingv.it/report/Rapporto_eruzione20021030.pdf.

Poliakov, A.N.B., Herrmann, H.J., 1994. Self organized criticality of plastic shear bands in rocks. Geophysical Research Letters 21, 2143–2146.

Pollard, D.D., Aydin, A., 1988. Progress in understanding jointing over the past century. Geological Society of America Bulletin 100, 1181–1204.

Rubin, A.M., Pollard, D.D., 1988. Dike-induced faulting in rift zones of Iceland and Afar. Geology 16, 413–417.

Rust, D., Neri, M., 1996. The boundaries of large-scale collapse on the flanks of Mount Etna, Sicily, in: McGuire, W.J., Jones, A.P., Neuberg, J. (Eds.), Volcano Instability on the Earth and Other Planets Geological Society of London Special Publication, 110, pp. 193–208.

Scholz, C.H., 1990. The Mechanics of Earthquake Faulting. Cambridge University Press, Cambridge.

Segall, P., Pollard, D.D., 1980. Mechanics of discontinuous faults. Journal of Geophysical Research 85, 4337–4350.

Sornette, D., Davy, P., 1991. Fault growth model and the universal fault length distribution. Geophysical Research Letters 18, 1079–1081.

Sylvester, A.G., 1988. Strike-slip faults. Geological American Society Bulletin 100, 1666–1703.

Tchalenko, J.S., 1970. Similarities between shear zones of different magnitudes. Geological Society of America Bulletin 81, 1625–1640.

Tibaldi, A., Groppelli, G., 2002. Volcano–tectonic activity along structures of the unstable NE flank of Mt. Etna (Italy) and their possible origin. Journal of Volcanology and Geothermal Research 115, 277–302.

Watterson, J., Walsh, J.J., Gillespie, A., Easton, S., 1996. Scaling systematics of fault sizes on a large-scale range fault map. Journal of Structural Geology 18, 199–214.

Willemse, E.J., 1997. Segmented normal faults: correspondence between three-dimensional mechanical models and field data. Journal of Geophysical Research 102, 675–692.